Article

Autofluorescence-Free Targeted Tumor Imaging Based on Luminous Nanoparticles with Composition-Dependent Size and Persistent Luminescence

Jie Wang, Qinqin Ma, Xiao-Xiao Hu, Haoyang Liu, Wei Zheng, Xueyuan Chen, Quan Yuan, and Weihong Tan

ACS Nano, **Just Accepted Manuscript** • DOI: 10.1021/acsnano.7b02643 • Publication Date (Web): 03 Aug 2017

Autofluorescence-Free Targeted Tumor Imaging Based on Luminous Nanoparticles with Composition-Dependent Size and Persistent Luminescence

Jie Wang,[†,§] Qinqin Ma,[†,§] Xiao-Xiao Hu,[‡] Haoyang Liu,[†] Wei Zheng,[⊥] Xueyuan Chen,[⊥] Quan Yuan,[,†] and Weihong Tan[‡]*

[†]Key Laboratory of Analytical Chemistry for Biology and Medicine (Ministry of Education), College of Chemistry and Molecular Sciences, Wuhan University, Wuhan 430072, China

[‡]Molecular Science and Biomedicine Laboratory, State Key Laboratory of Chemo/Biosensing and Chemometrics, College of Chemistry and Chemical Engineering, Hunan University, Changsha 410082, China

[⊥]CAS Key Laboratory of Design and Assembly of Functional Nanostructures, Fujian Institute of Research on the Structure of Matter, Chinese Academy of Sciences, Fuzhou, Fujian 350002, China

ABSTRACT

Optical bioimaging is an indispensable tool in modern biology and medicine, but the technique is susceptible to autofluorescence interference. Persistent nanophosphors provide an easy-to-perform and highly efficient mean to eliminate tissue autofluorescence. However, direct synthesis of persistent nanophosphors with tunable properties to meet different bioimaging requirements remains largely unexplored. In this work, zinc gallogermanate ($Zn_{1+x}Ga_{2-2x}Ge_xO_4$:Cr, $0 \leq x \leq 0.5$, ZGGO:Cr) persistent luminescence nanoparticles with composition-dependent size and persistent luminescence are reported. The size of the ZGGO:Cr nanoparticles gradually increases with the raise of x in the chemical formula. Moreover, the intensity and decay time of persistent luminescence in ZGGO:Cr nanoparticles can also be fine-tuned by simply changing x in the formula. *In vivo* bioimaging tests demonstrate that ZGGO:Cr nanoparticles can efficiently eliminate tissue autofluorescence, and the nanoparticles also show good promise in long-term bioimaging since they can be easily reactivated *in vivo*. Furthermore, an aptamer-guided ZGGO:Cr bioprobe is constructed and it displays excellent tumor-specific accumulation. The ZGGO:Cr nanoparticles are ideal for autofluorescence-free targeted bioimaging, indicating their great potential in monitoring cellular networks and construction of guiding systems for surgery.

KEYWORDS: persistent luminescence, bioimaging, autofluorescence, aptamer, near-infrared light, nanoparticle

Optical bioimaging has revolutionized modern biology and medicine by providing optical, thus spatially and temporally precise, ways to decode molecular and cellular behaviors in their native contexts.[1-3] Optical bioimaging provides benefits such as high sensitivity, non-invasiveness and easy operation on readily available instruments.[4-7] Despite the many merits, this technique still faces challenges, most notably tissue autofluorescence interference.[8,9] To overcome this obstacle, several kinds of fluorescent materials were employed,[10] such as near-infrared (NIR)-activatable phosphors[11-13] and long-lifetime phosphors.[14] Studies on clinical samples reported that some chromophores in tissue,[15] such as cutaneous melanin,[16] showed autofluorescence even under NIR light excitation, which inevitably compromises the effectiveness of NIR-activatable phosphors in avoiding autofluorescence. On the other hand, the application of long lifetime phosphors is usually hindered by the need for complicated and expensive time-resolved instruments.[17] Therefore, developing phosphors that can efficiently eliminate autofluorescence in an easily performed manner is still in urgent need.

Persistent luminescence refers to the phenomenon whereby luminescence remains after the cessation of excitation.[18,19] As the lifetimes of biological chromophores are in the range of nanoseconds, tissue autofluorescence can be easily avoided by collecting the persistent luminescence signal after the short-lived autofluorescence has decayed completely.[20-26] In past years, superior sensitivity and signal-to-noise ratio have been obtained in bioimaging with persistent luminescence nanoparticles (PLNPs) due to the efficient elimination of autofluorescence interference.[27-33] Besides, PLNPs, especially visible-light-activatable PLNPs, are ideal candidates for long-term bioimaging, since they can be directly recharged *in vivo*.[34-36] Although PLNPs provide many advantages, considerable challenges still have to be overcome in their biomedical applications.[20] Usually, PLNPs are prepared by top-down methods like

grinding, which produce water-insoluble particles with uncontrollable size and shape.[20] Controlled synthesis of PLNPs remains largely unexplored at present,[37,38] and the lack of PLNPs with controllable properties (size, luminescence, surface functionalization, etc.) inevitably sets significant limitations on the biomedical applications of PLNPs. Consequently, developing PLNPs with tunable properties to meet different biomedical requirements is highly desired.

Herein, we report the direct synthesis of zinc gallogermanate PLNPs ($Zn_{1+x}Ga_{2-2x}Ge_xO_4$:Cr, $0 \leqslant x \leqslant 0.5$, ZGGO:Cr) with composition-dependent size and persistent luminescence. The size and persistent luminescence of the ZGGO:Cr nanoparticles can be fine-tuned by simply changing x in the chemical formula. The ZGGO:Cr nanoparticles can efficiently avoid tissue autofluorescence since they can remain luminescent after excitation ceases, and the nanoparticles also display special advantages in long-term bioimaging due to their long persistent luminescence. An aptamer-guided ZGGO:Cr bioprobe was further constructed and it showed significantly improved tumor accumulation and retention. The developed ZGGO:Cr nanoparticles provides ideal candidates for autofluorescence-free bioimaging and can be further applied to potential areas such as real-time monitoring of biological processes and constructing guiding systems for surgery.

RESULTS AND DISCUSSION

All of the $Zn_{1+x}Ga_{2-2x}Ge_xO_4$:Cr ($0 \leq x \leq 0.5$) nanoparticles were prepared by a hydrothermal method. The size and crystal structure of the nanoparticles were studied using transmission electron microscopy (TEM) and X-ray powder diffraction (XRD) measurements. As shown in Figure 1a and Figure S1, all of the ZGGO:Cr nanoparticles are well-dispersed with uniform shape and size. The size of the ZGGO:Cr nanoparticles gradually increases as the value of x in the chemical formula increases. Energy-dispersive X-ray analysis shows the presence of Zn, Ga,

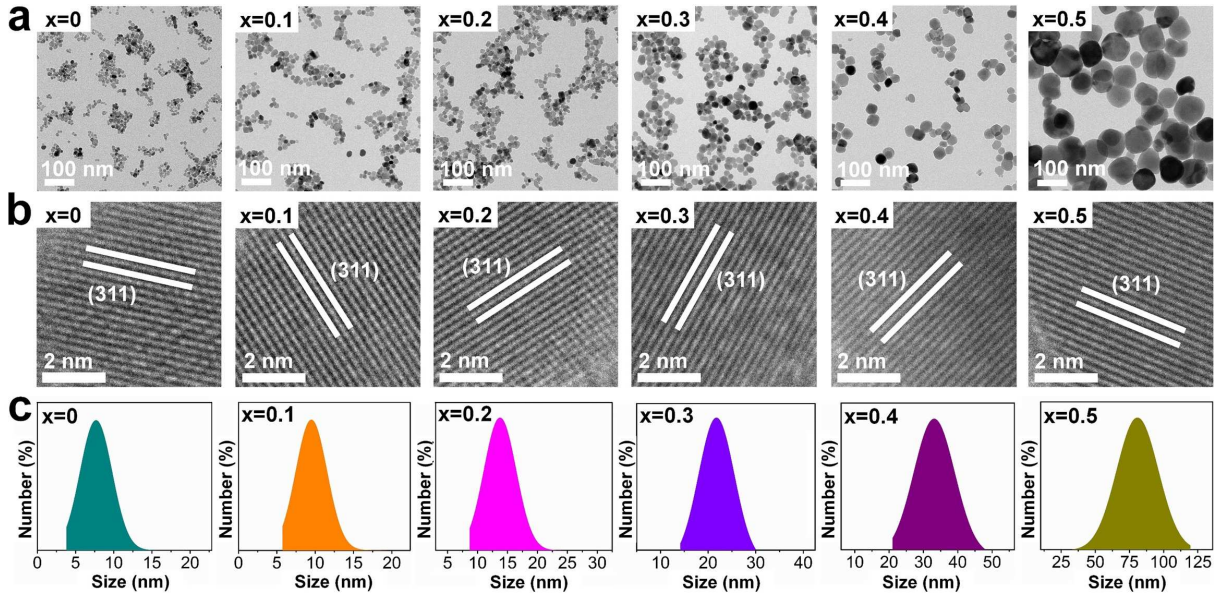

Figure 1. TEM images (a), HRTEM images (b) and (c) corresponding size distributions of the $Zn_{1+x}Ga_{2-2x}Ge_xO_4$:Cr nanoparticles with x from 0 to 0.5.

Ge, O and Cr in the ZGGO:Cr nanoparticles (Figure S2). XRD measurements (Figure S3) further indicated that all of the ZGGO:Cr nanoparticles are highly crystalline with typical cubic spinel structure (JCPDS file number 38-1240), indicating the formation of a homogeneous $Zn_{1+x}Ga_{2-2x}Ge_xO_4$:Cr solid state solution. High-resolution TEM (HRTEM) images of the ZGGO:Cr nanoparticles (Figure 1b) with different chemical composition display lattices corresponding to the (311) spacing of the cubic spinel. The size distributions of the ZGGO:Cr nanoparticles were further determined and are shown in Figure 1c and Figure S4. It is clear that the size of the ZGGO:Cr nanoparticles increases from about 7 nm to around 80 nm with increasing x in the formula from 0 to 0.5. Further increasing x to 0.6 leads to the formation of a $ZnGa_2O_4$ and Zn_2GeO_4 mixture (Figure S5, S6). The above results clearly show that the sizes of the $Zn_{1+x}Ga_{2-2x}Ge_xO_4$:Cr nanoparticles can be fine controlled by simply tuning the chemical composition.

Efficient visible light activation of persistent phosphors is crucial for long-term bioimaging to ensure *in vivo* recovery of persistent luminescence to increase imaging sensitivity and signal-to-

noise ratio.[24] The visible light-activated persistent luminescence in $Zn_{1+x}Ga_{2-2x}Ge_xO_4$:Cr ($0 \leq x \leq 0.5$) nanoparticles was further investigated. The excitation spectrum of the ZGGO:Cr nanoparticles shows the typical excitation bands of Cr^{3+} in the visible region (Figure S7).[34] The steady-state emission spectrum of ZGGO:Cr nanoparticles under visible light excitation (550 nm) is shown in Figure 2a. For all of the ZGGO:Cr nanoparticles, the spectrum is composed of zero photon lines (R and N2) and Stokes phonon side bands (S-PSB).[39] The R and S-PSB bands are ascribed to Cr^{3+} ions with an ideal octahedral environment (Cr_R), while the N2 line is indexed to Cr^{3+} ions in an octahedral environment distorted by neighboring charge defects (Cr_{N2}),[40] as labeled in Figure 2a. The intensity of the R and S-PSB bands gradually decreases and the N2 line dominates the spectrum with increasing x, suggesting an increase of Cr_{N2} in the ZGGO:Cr nanoparticles. Previous studies have demonstrated that Cr_{N2} is the dominant contributor to persistent luminescence in Cr^{3+} doped zinc gallate,[39,40] thus the increased Cr_{N2} ratio indicates a significant change of persistent luminescence in ZGGO:Cr nanoparticles. The persistent luminescence decay in $Zn_{1+x}Ga_{2-2x}Ge_xO_4$:Cr ($0 \leq x \leq 0.5$) nanoparticles was further measured with pre-excitation by a commercial orange LED (1000 lumen), as shown in Figure 2b. All of the ZGGO:Cr nanoparticles are efficiently activated and strong persistent luminescence is clearly observed after removal of the LED. The persistent luminescence intensity and decay time first increase and then decrease with increasing x from 0 to 0.5. It is noteworthy that the ZGGO:Cr nanoparticles with x = 0.2 display strong persistent luminescence even after 10 h of decay, suggesting their good promise in long-term bioimaging. Additionally, the decay and reactivation circulation of the ZGGO:Cr (x = 0.2) nanoparticles was measured (Figure S8). During the ten cycles, no obvious changes of the persistent luminescence decay in ZGGO:Cr (x = 0.2) nanoparticles are observed, suggesting that the ZGGO:Cr nanoparticles possess good

photostability. The above results thus clearly demonstrated that $Zn_{1+x}Ga_{2-2x}Ge_xO_4$:Cr PLNPs with composition-dependent size and persistent luminescence have been successfully developed and can be further utilized to meet different requirements in biomedical applications.

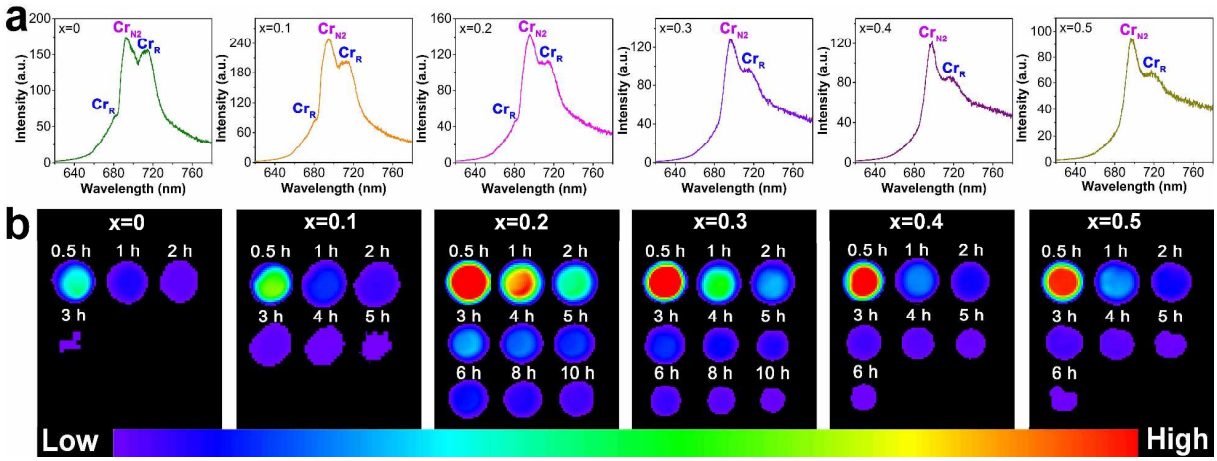

Figure 2. Photoluminescence spectrum (a) and persistent luminescence decay images (b) of the $Zn_{1+x}Ga_{2-2x}Ge_xO_4$:Cr nanoparticles with x from 0 to 0.5.

The capability of the developed ZGGO:Cr nanoparticles to eliminate tissue autofluorescence was further investigated. Tissue autofluorescence decays rapidly after excitation cease due to its short lifetime, while ZGGO:Cr nanoparticles can remain luminescent after the stoppage of excitation (Figure S9). Thus autofluorescence interference can be avoided by collecting the persistent luminescence signal of ZGGO:Cr nanoparticle after autofluorescence decays completely. As illustrated in Figure 3a, ZGGO:Cr nanoparticles were injected into mice and the nanoparticles were directly activated *in vivo*. The mouse displays strong autofluorescence under excitation, which seriously decreases the imaging sensitivity and signal-to-noise ratio. However, after the removal of the excitation source, the tissue autofluorescence disappeared rapidly but the persistent luminescence signal remained, leading to efficient elimination of autofluorescence interference. In this study, trace amounts of ZGGO:Cr (x = 0.2) nanoparticles were subcutaneously injected into mice and were further activated *in vivo* with an orange LED. The

luminescence signal of the injected nanoparticles was captured with an IVIS Lumina XR Imaging System after the removal of LED excitation. In addition, a cyanine-derivative dye (λ_{Em} = 670 nm, Figure S10a) and Ag_2Se (λ_{Em} = 740 nm, Figure S10b) were also subcutaneously injected into mice for comparison. As shown in Figure 3b (left panel), the emission signal from the injected ZGGO:Cr nanoparticles is clearly visualized without any autofluorescence interference. As for cyanine-derivative dye (middle panel) and Ag_2Se (right panel) injected mice, strong autofluorescence is observed and the emission signal of the injected cyanine-derivative dye or Ag_2Se can hardly be distinguished. These images clearly show the potent ability of ZGGO:Cr nanoparticles in eliminating autofluorescence interference.

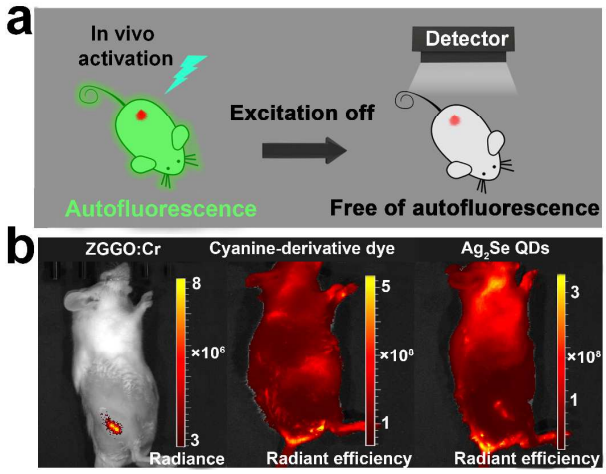

Figure 3. (a) Elimination of autofluorescence interference with ZGGO:Cr nanoparticles. (b) *In vivo* mice imaging with ZGGO:Cr (x = 0.2) nanoparticles, cyanine-derivative dye and Ag_2Se. The injected dosage of ZGGO:Cr (x = 0.2), cyanine-derivative dye and Ag_2Se is kept as 1 μg.

Since the ZGGO:Cr nanoparticles can be efficiently activated by an orange LED, the persistent luminescence of injected nanoparticles can be easily recovered whenever needed. The *in vivo* reactivation and long-term bioimging potential of the ZGGO:Cr nanoparticles were further tested. The ZGGO:Cr (x = 0.2) nanoparticles were subcutaneously injected into mice and were further activated *in vivo* with an LED. As shown in Figure 4a, the emission signal from the

injected ZGGO:Cr nanoparticles is clearly observed and luminescence remains even after 1 h of decay. The injected nanoparticles were further reactivated *in vivo* with the LED and decay images are shown in Figure 4b. Bright luminescence from the ZGGO:Cr nanoparticles is observed, suggesting that the nanoparticles can be efficiently reactivated *in vivo*. The luminescence signal also remains after 1 h of decay. The third *in vivo* reactivation gives similar decay images (Figure 4c). Moreover, compared to the former two groups, no obvious decrease of luminescence intensity is observed at the same time point, suggesting the good photostability of the ZGGO:Cr nanoparticles. The above *in vivo* reactivation tests clearly demonstrated that persistent luminescence of the ZGGO:Cr nanoparticles can remain for more than 1 h and can further be efficiently recovered with an orange LED, making the ZGGO:Cr nanoparticles valuable in long-term bioimaging.

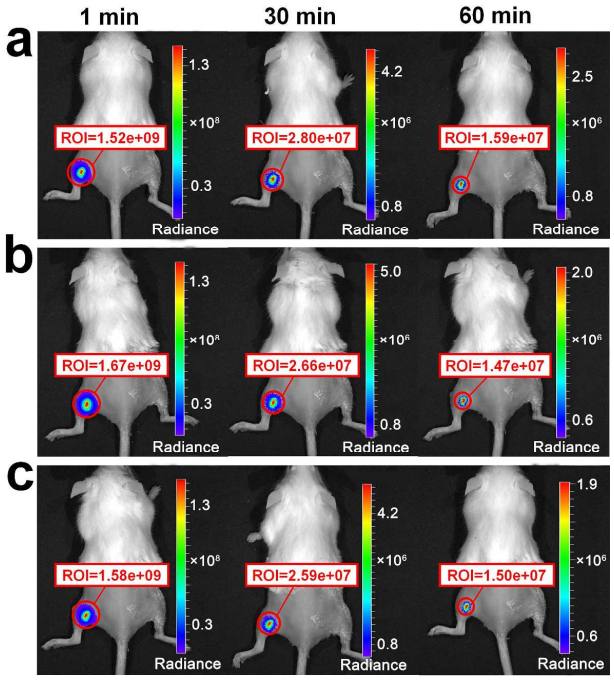

Figure 4. (a) *In vivo* imaging of normal mice after subcutaneous injection of ZGGO:Cr (x = 0.2) nanoparticles. Decay images after the second (b) and third (c) *in vivo* activation.

The ZGGO:Cr nanoparticles were directly synthesized by a hydrothermal method, which ensures good dispersability and abundant surface functional groups for bioconjugation. As illustrated in Figure 5a, the ZGGO:Cr were further functionalized with DNA aptamer (ZGGO:Cr-Apt) for targeted bioimaging. The 4T1 murine breast cancer cells and a G-rich DNA

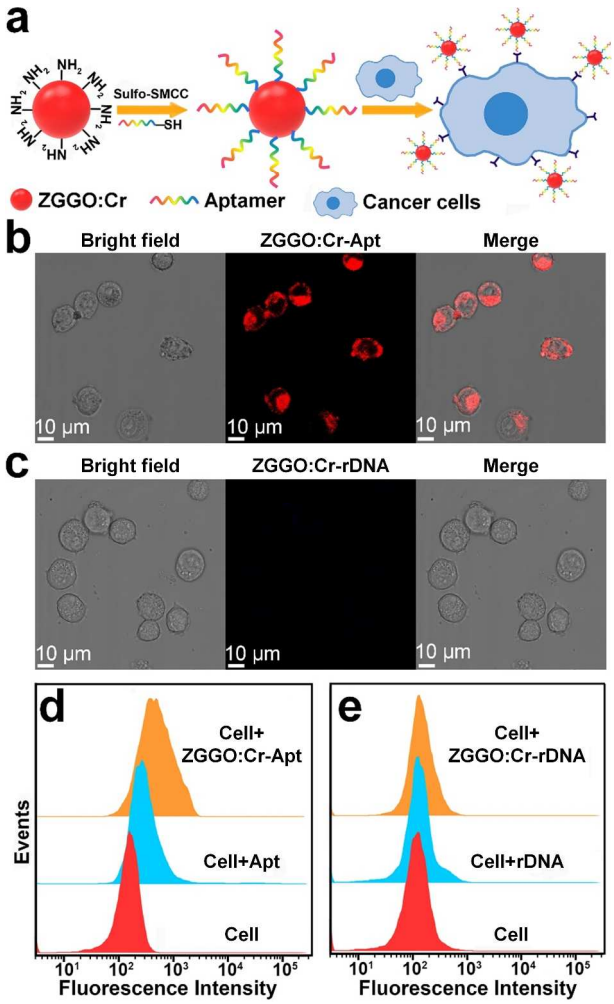

Figure 5. (a) Construction of ZGGO:Cr-Apt probe for recognition of target cancer cells. Confocal microscopy images of 4T1 cells treated with ZGGO:Cr-Apt (b) and ZGGO:Cr-rDNA (c). The emission signal is from the nanoparticles upon excitation with a 405 nm laser. Flow cytometry histograms to monitor the binding of ZGGO:Cr-Apt (d) and ZGGO:Cr-rDNA (e) with 4T1 cells. The emission signal is from the FITC labeled on aptamer and random DNA molecules.

aptamer targeting 4T1 cells were employed as the model.[41] For comparison, a random DNA (rDNA) molecule was also grafted to the surface of ZGGO:Cr nanoparticles (ZGGO:Cr-rDNA) for bioimaging tests. Zeta potential measurements suggest that DNA aptamer is successfully conjugated to the surface of ZGGO:Cr nanoparticles (Figure S11), and the hydrodynamic diameter of the ZGGO:Cr nanoparticles is about 50 nm (Figure S12). Cell cytotoxicity assay further shows that the ZGGO:Cr-Apt nanoparticles possess good biocompatibility (Figure S13). The binding of the ZGGO:Cr-Apt probe and ZGGO:Cr-rDNA to target cancer cells was investigated with confocal microscopy and flow cytometry. As shown in Figure 5b and Figure S14, strong emission signal was detected in 4T1 cells after incubation with the ZGGO:Cr-Apt probe. Overlays of dark-field and bright field images demonstrate that the signal was primarily within the cytoplasm, indicating the aptamer-mediated internalization of the probe into 4T1 cells. In contrast, no obvious emission signal was observed in 4T1 cells treated with the ZGGO:Cr-rDNA, suggesting that ZGGO:Cr-rDNA displays little binding affinity to 4T1 cells. Flow cytometry results are presented in Figure 5d and 5e. A large fluorescence peak shift is observed for 4T1 cells incubated with the ZGGO:Cr-Apt probe, clearly indicating the strong binding affinity of the probe to target cells (Figure 5d). However, both rDNA and ZGGO:Cr-rDNA exhibit weak affinity to 4T1 cells, as evidenced by the small fluorescence peak shifts (Figure 5e). These results thus clearly demonstrate the aptamer-guided binding of the ZGGO:Cr-Apt probe to target cells.

The ZGGO:Cr-rDNA and ZGGO:Cr-Apt were further injected into 4T1 tumor-bearing mice through tail vein to investigate tumor-specific accumulation capability. For mice injected with ZGGO:Cr-rDNA (Figure 6a), the luminescence signal was observed at the tumor site within 10

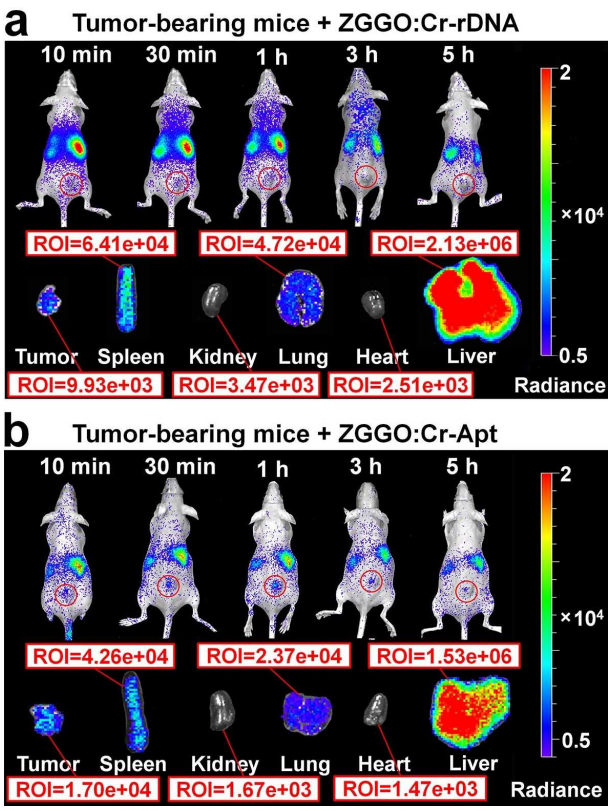

Figure 6. *In vivo* and *ex vivo* luminescent images of 4T1 tumor-bearing mice after intravenous injection of ZGGO:Cr-rDNA (a) and ZGGO:Cr-Apt (b) nanoparticles.

min, due to the enhanced permeability and retention effect in tumor vasculature. The luminescence signal at the tumor site almost disappears at 3 h. In contrast, ZGGO:Cr-Apt probe displays significantly improved tumor-targeting capability. As shown in Figure 6b, a noticeable emission signal was observed in tumor sites within 10 min. The signal intensity reached a maximum at 1 h and then decreased gradually. It is noteworthy that the emission signal from the tumor site is still clearly visualized at 5 h. Mice injected with the ZGGO:Cr-Apt probe were sacrificed after 1 h of postinjection, and the *ex vivo* images of the various organs and tumor are presented. Strong emission appears in the tumor tissue, suggesting the efficient accumulation of the probe in tumor tissue. The relative distribution of the ZGGO:Cr-rDNA and ZGGO:Cr-Apt nanoparticles in the isolated tumor and organs (Figure S15) further indicates the efficient

accumulation of ZGGO:Cr-Apt nanoparticles in tumor. The above results clearly demonstrated that the bioimaging probe possesses better tumor accumulation capability and longer tumor retention than ZGGO:Cr-rDNA, and this can be ascribed to the strong binding affinity of DNA aptamer to their target cells.[42,43] Additionally, the biocompatibility of the ZGGO:Cr-Apt was systematically investigated. The body weights of healthy Kunming mice injected with ZGGO:Cr-Apt nanoparticles show no obvious difference to that of mice injected with PBS buffer (Figure S16). Most of the injected ZGGO:Cr-Apt nanoparticles can be cleared from mice after 24 h of postinjection (Figure S17), and almost complete amount of ZGGO:Cr-Apt nanoparticles were cleared from mice after 3 weeks of postinjection (Figure S18). Blood biochemistry and hematology examinations (Figure S19) show that the liver function indexes, kidney function indicators, and blood indexes of mice injected with the ZGGO:Cr-Apt have no significant differences compared with the control group. The lethal dose 50 (LD_{50}) examinations suggest that the LD_{50} value of the ZGGO:Cr-Apt nanoparticles is higher than 2000 mg/kg (Table S1). These results clearly show that the ZGGO:Cr-Apt nanoparticles possess good biocompatibility. As a result, the ZGGO:Cr-rDNA probe holds good promise in areas such as cancer diagnosis and deciphering specific cellular networks.

CONCLUSIONS

In this work, we have presented the composition-dependent properties of ZGGO:Cr nanoparticles and their excellent performance in bioimaging. The ZGO:Cr nanoparticles were directly synthesized *via* a hydrothermal method. The size of the ZGGO:Cr nanoparticles can be fine-tuned from sub 10 nm to about 80 nm. In addition, the persistent luminescence intensity and decay time can also be fine-tuned by simply changing the chemical composition of the nanoparticles. *In vivo* mice imaging tests demonstrated that ZGGO:Cr nanoparticles can

efficiently eliminate tissue autofluorescence interference and are ideal for long-term bioimaging. Furthermore, aptamer-guided ZGGO:Cr nanoparticles showed significantly improved tumor specific accumulation ability and long tumor retention, making them valuable in cancer diagnosis. To conclude, the developed ZGGO:Cr nanoparticles are ideal for autofluorescence-free targeted bioimaging over a long period, and they can further contribute to areas such as the study of complex molecular networks and construction of guiding systems for surgery.

EXPERIMENTAL SECTION

Preparation of $Zn_{1+x}Ga_{2-2x}Ge_xO_4$:Cr ($0 \le x \le 0.5$) nanoparticles. The synthesis of ZGGO:Cr nanoparticles with composition of x = 0.1 is used as an example. Typically, 1.1 mmol $Zn(NO_3)_2$, 1.8 mmol $Ga(NO_3)_3$, 0.1 mmol Na_2GeO_3, 0.0075 mmol $Cr(NO_3)_3$ were dissolved in 11 mL deionized water. Then, ammonium hydroxide (28%, wt) was quickly added to the above solution to adjust the pH value to around 8.5 with vigorous stirring. Then the mixture was left stirring for 1 h at room temperature. After that, the solution was transferred to a Teflon-lined autoclave and reacted at 220 $^{\circ}$C for 6 h. The as-prepared ZGGO:Cr nanoparticles were collected by centrifugation and washed 3 times with deionized water. The remaining ZGGO:Cr nanoparticles were synthesized with corresponding amounts of $Zn(NO_3)_2$, $Ga(NO_3)_3$, and Na_2GeO_3 precursors according to the above procedure.

Measuring the persistent luminescence in ZGGO:Cr nanoparticles. The ZGGO:Cr nanoparticles with different compositions were placed in a 24-well-plate. Then the nanoparticles were illuminated with a commercial orange LED (1000 lumen) for 5 min and put into an IVIS Lumina XR Imaging System to record the decay images. The exposure time was set at 5 s.

Autofluorescence-free bioimaging study. Healthy Kunming mice were purchased from Hubei Provincial Academy of Preventive Medicine (Wuhan, China). The ZGGO:Cr

nanoparticles (x = 0.2), cyanine-derivative dye and Ag_2Se (1 μg in 30 μL) were subcutaneously injected into mice, respectively. The ZGGO:Cr injected mice were illuminated with the LED for 2 min before capturing the luminescence images with an IVIS Lumina XR Imaging System in the bioluminescence mode. The fluorescence images of the cyanine-derivative dye and Ag_2Se injected mice were obtained with the IVIS Lumina XR Imaging System in the fluorescence mode**.**

Long-term bioimaging study. In a typical experiment, ZGGO:Cr nanoparticles (x = 0.2, 40 μL, 3 mg mL^{-1}) were subcutaneously injected into healthy Kunming mice at the left leg. Then the LED was applied to activate the injected nanoparticles for 2 min and the mice were immediately placed in the imaging system to record the decay images. After 1 h of decay, the mice were again illuminated with the orange LED for 2 min, and the persistent luminescence images within 1 h were recorded. The exposure time was set at 5 s.

Preparation of ZGGO:Cr-Apt and ZGGO:Cr-rDNA. Amino groups were first conjugated to the surface of ZGGO:Cr nanoparticles (ZGGO:Cr-NH_2) by the hydrolysis of APTES according to the protocol reported in previous studies.[21,31,34] Briefly, 50 mg of ZGGO:Cr nanoparticles (x = 0.2) was dispersed in 20 mL of dimethylformamide (DMF) by sonication. Then 200 μL of APTES was added dropwise to the nanoparticle solution under vigorous stirring. The reaction mixture was kept at 80 °C for 12 h with vigorous stirring. The obtained ZGGO:Cr-NH_2 nanoparticles were washed with DMF three times and further dispersed in 25 mL deionized water. The ZGGO:Cr-Apt nanoparticles were further prepared according to a previously reported method.[44,45] Typically, ZGGO:Cr-NH_2 nanoparticles (1 mg) were dispersed in 1 mL HEPES buffer (10 mM, pH = 7.2) by sonication. Then 0.2 mg Sulfo-SMCC was added to the nanoparticle dispersion. The resultant mixture was kept at 25 °C for 0.5 h with shaking. Then, the

maleimide-activated nanoparticles were recovered by centrifugation and re-dispersed in 1 mL Tris-HCl buffer containing 2 nmol DNA aptamer. The solution was allowed to react at 25 °C for 12 h. Afterwards, the as-prepared ZGGO:Cr-Apt nanoparticles were collected by centrifugation and the free aptamer was removed by washing three times with Tris-HCl buffer. The ZGGO:Cr-rDNA were prepared by the same procedure.

Cell cytotoxicity assay. The 4T1 cells (1×10^5 well^{-1} in 180 μL of cell culture medium) were seeded into a 96-well cell-culture plate. Then ZGGO:Cr-Apt in PBS buffer (20 μL) with desired concentrations was added to the test well. The resultant cell mixture was incubated normally for 48 h and a standard MTT assay was further applied to measure the viability of cells.

Targeted cell imaging. The ZGGO:Cr-Apt and ZGGO:Cr-rDNA (100 μL, 1 mg mL^{-1}) were co-incubated with 4T1 cells (0.5 mL, 1×10^5 mL^{-1}) at 37 °C in binding buffer for 2 h. Then the cells were centrifuged and washed three times with washing buffer to remove the free ZGGO:Cr-Apt or ZGGO:Cr-rDNA nanoparticles. The resultant cells were dispersed in 500 μL binding buffer and subjected to confocal fluorescence microscopy analysis.

Flow cytometric analysis. Typically, FITC labeled DNA aptamer (20 μL, 10 μM), ZGGO:Cr-Apt probe (200 μL, 1 mg mL^{-1}), FITC labeled rDNA and ZGGO:Cr-rDNA nanoparticles were co-incubated with 4T1 cells (0.5 mL, 1×10^6 mL^{-1}) at 4 °C in binding buffer for 1 h. The cells were centrifuged and washed three times with washing buffer. The resultant cells were re-dispersed in 500 μL of binding buffer and further subjected to flow cytometry analysis by counting 10000 events.

***In vivo* cytotoxicity study.** Healthy Kunming mice (~25 g) were intravenously injected with ZGGO:Cr-Apt dispersion at the desired dose (0 mg kg^{-1}, 10 mg kg^{-1}, 25 mg kg^{-1}, 50 mg kg^{-1}). The body weights of the mice were recorded within the following 1 month as an indicator for

studying toxic effects of the ZGGO:Cr-Apt probe.

Biodistribution study. The ZGGO:Cr-Apt (150 μL, 2 mg mL^{-1}) was injected through the tail vein into healthy Kunming mice. The luminescence images of the mice were recorded with the imaging system within 12 h. Mice were sacrificed 24 h post-injection, and *ex vivo* luminescence images of the various organs were recorded. The mice and isolated organs were illuminated with the orange LED for 2 min before capturing the luminescence images. The exposure time was set to 60 s.

Blood biochemistry and hematology examinations. Healthy Kunming mice were injected with the ZGGO:Cr-Apt nanoparticles at different doses (0, 10, 25, 50 mg/kg) through the tail vein (n = 4 in each group). The blood of mice were collected after 3 weeks of postinjection. The blood biochemistry and hematology examinations were conducted on an automatic biochemical analyzer and an automatic blood cell analyzer, respectively.

Lethal dose 50 (LD_{50}) study. Healthy Kunming mice were intravenously injected with ZGGO:Cr-Apt saline solution at different doses (0, 50, 250, 500, 1000, 2000 mg/kg, n = 8 in each group). The mice were observed for 2 weeks after the injection. The number of dead mice in each group were recorded.

***In vivo* targeted tumor imaging.** Briefly, ZGGO:Cr-rDNA and ZGGO:Cr-Apt (150 μL, 2 mg mL^{-1}) were injected through the tail vein into 4T1-tumor bearing mice. The luminescence images of the mice were recorded with the imaging system. Mice injected with ZGGO:Cr-Apt were sacrificed 1 h postinjection, and *ex vivo* luminescence images of the isolated organs and tumor tissue were captured. The parameters for *in vivo* mice imaging and *ex vivo* organ imaging were similar to those in the biodistribution study.

ASSOCIATED CONTENT

Supporting Information.

TEM images, EDX measurements, XRD measurements, excitation spectrum of the ZGGO:Cr nanoparticles, and bioimaging images are provided. This material is available free of charge via the Internet at http://pubs.acs.org. This material is available free of charge *via* the Internet at http://pubs.acs.org.

AUTHOR INFORMATION

Corresponding Author

*E-mail: yuanquan@whu.edu.cn

Author Contributions

The manuscript was written through contributions of all authors. All authors have given approval to the final version of the manuscript. §Jie Wang and Qinqin Ma contributed equally.

Notes

The authors declare no competing financial interest.

ACKNOWLEDGMENT

This work was supported by the National Natural Science Foundation of China (21422105, 21675120), Ten Thousand Talents Program for Young Talents, the CAS Cross-Disciplinary & Collaborative Research Team Program, and the CAS/SAFEA International Partnership Program for Creative Research Teams.

REFERENCES

(1) Zagorovsky, K.; Chan, W. C. Bioimaging: Illuminating the Deep. *Nat. Mater.* **2013**, *12*, 285–287.

(2) Dai, Y. L.; Ma, P. A.; Cheng, Z. Y.; Kang, X. X.; Zhang, X.; Hou, Z. Y.; Li, C. X.; Yang, D. M.; Zhai, X. F.; Lin, J. Upconversion Cell Imaging and pH-Induced Thermally Controlled Drug Release from $NaYF_4$:Yb^{3+}/Er^{3+}@Hydrogel Core–Shell Hybrid Microspheres. *ACS Nano* **2012**, *6*, 3327–3338.

(3) Vahrmeijer, A. L.; Hutteman, M.; van der Vorst, J. R.; van de Velde, C. J.; Frangioni, J. V. Image–Guided Cancer Surgery Using Near-Infrared Fluorescence. *Nat. Rev. Clin. Oncol.* **2013**, *10*, 507–518.

(4) Yang, Y.; Zhao, Q.; Feng, W.; Li, F. Luminescent Chemodosimeters for Bioimaging. *Chem. Rev.* **2013**, *113*, 192–270.

(5) Xu, H.; Li, Q.; Wang, L. H.; He, Y.; Shi, J. Y.; Tang, B.; Fan, C. H. Nanoscale Optical Probes for Cellular Imaging. *Chem. Soc. Rev.* **2014**, *43*, 2650–2661.

(6) Zhao, Q.; Huang, C.; Li, F. Phosphorescent Heavy-Metal Complexes for Bioimaging. *Chem. Soc. Rev.* **2011**, *40*, 2508–2524.

(7) Ma, P. A.; Xiao, H. H.; Li, X. X.; Li, C. X.; Dai, Y. L.; Cheng, Z. Y.; Jing, X. B.; Lin, J. Rational Design of Multifunctional Upconversion Nanocrystals/Polymer Nanocomposites for Cisplatin (IV) Delivery and Biomedical Imaging. *Adv. Mater.* **2013**, *25*, 4898–4905.

(8) Smith, A. M.; Mancini, M. C.; Nie, S. Second Window for *In Vivo* Imaging. *Nat. Nanotechnol.* **2009**, *4*, 710–711.

(9) Berezin, M. Y.; Achilefu, S. Fluorescence Lifetime Measurements and Biological Imaging. *Chem. Rev.* **2010**, *110*, 2641–2684.

(10) Guo, Z.; Park, S.; Yoon, J.; Shin, I. Recent Progress in the Development of Near–Infrared Fluorescent Probes for Bioimaging Applications. *Chem. Soc. Rev.* **2014**, *43*, 16–29.

(11) Zhou, J.; Liu, Z.; Li, F. Upconversion Nanophosphors for Small–Animal Imaging. *Chem. Soc. Rev.* **2012**, *41*, 1323–1349.

(12) Zhou, B.; Shi, B.; Jin, D.; Liu, X. Controlling Upconversion Nanocrystals for Emerging Applications. *Nat. Nanotechnol.* **2015**, *10*, 924–936.

(13) Yang, D. M.; Dai, Y. L.; Liu, J. H.; Zhou, Y.; Chen, Y. Y.; Li, C. X.; Ma, P. A.; Lin, J. Ultra–Small $BaGdF_5$-Based Upconversion Nanoparticles as Drug Carriers and Multimodal Imaging Probes. *Biomaterials* **2014**, *35*, 2011–2023.

(14) Zheng, W.; Zhou, S.; Chen, Z.; Hu, P.; Liu, Y.; Tu, D.; Zhu, H.; Li, R.; Huang, M.; Chen, X. Sub–10 nm Lanthanide–Doped CaF_2 Nanoprobes for Time–Resolved Luminescent Biodetection. *Angew. Chem. Int. Ed.* **2013**, *52* , 6671–6676.

(15) Wang, S.; Zhao, J.; Lui, H.; He, Q.; Zeng, H. *In Vivo* Near–Infrared Autofluorescence Imaging of Pigmented Skin Lesions: Methods, Technical Improvements and Preliminary Clinical Results. *Skin Research and Technology* **2013**, *19*, 20–26.

(16) Huang, Z.; Zeng, H.; Hamzavi, I.; Alajlan, A.; Tan, E.; McLean, D. I.; Lui, H. Cutaneous Melanin Exhibiting Fluorescence Emission under Near-Infrared Light Excitation. *J. Biomed. Opt.* **2006**, *11*, 034010–034016.

(17) Tu, D.; Liu, L.; Ju, Q.; Liu, Y.; Zhu, H.; Li, R.; Chen, X. Time–Resolved FRET Biosensor Based on Amine–Functionalized Lanthanide–Doped $NaYF_4$ Nanocrystals. *Angew. Chem. Int. Ed.* **2011**, *50*, 6306–6310.

(18) Li, Y.; Gecevicius, M.; Qiu, J. Long Persistent Phosphors–from Fundamentals to Applications. *Chem. Soc. Rev.* **2016**, *45*, 2090–2136.

(19) Pan, Z.; Lu, Y. Y.; Liu, F. Sunlight-Activated Long-Persistent Luminescence in the Near–Infrared from Cr^{3+}–doped Zinc Gallogermanates. *Nat. Mater.* **2012**, *11*, 58–63.

(20) Li, N.; Li, Y.; Han, Y.; Pan, W.; Zhang, T.; Tang, B. A Highly Selective and Instantaneous Nanoprobe for Detection and Imaging of Ascorbic Acid in Living Cells and *In Vivo*. *Anal. Chem.* **2014**, *86*, 3924–3930.

(21) de Chermont, Q. l. M.; Chanéac, C.; Seguin, J.; Pellé, F.; Maîtrejean, S.; Jolivet, J. P.; Gourier, D.; Bessodes, M.; Scherman, D. Nanoprobes with Near–Infrared Persistent Luminescence for *In Vivo* Imaging. *Proc. Natl. Acad. Sci. U. S. A.* **2007**, *104*, 9266–9271.

(22) Song, L.; Lin, X. H.; Song, X. R.; Chen, S.; Chen, X. F.; Li, J.; Yang, H. H. Repeatable Deep–Tissue Activation of Persistent Luminescent Nanoparticles by Soft X–Ray for High Sensitivity Long–Term *In Vivo* Bioimaging. *Nanoscale* **2017**, *9*, 2718–2722.

(23) Li, N.; Diao, W.; Han, Y.; Pan, W.; Zhang, T.; Tang B. MnO_2–Modified Persistent Luminescence Nanoparticles for Detection and Imaging of Glutathione in Living Cells and *In Vivo*. *Chem. - Eur. J.* **2014**, *20*, 16488–16491.

(24) Li, Z.; Zhang, Y.; Wu, X.; Wu, X.; Maudgal, R.; Zhang, H.; Han, G. *In Vivo* Repeatedly Charging Near–Infrared–Emitting Mesoporous $SiO_2/ZnGa_2O_4:Cr^{3+}$ Persistent Luminescence Nanocomposites. *Adv. Sci.* **2015**, *2*, 1500001.

(25) Zhang, L.; Lei, J.; Liu, J.; Ma, F.; Ju, H. Persistent Luminescence Nanoprobe for Biosensing and Lifetime Imaging of Cell Apoptosis *via* Time–Resolved Fluorescence Resonance Energy Transfer. *Biomaterials* **2015**, *67*, 323–334.

(26) Li, Z. J.; Huang, L.; Zhang, Y. W.; Zhao, Y.; Yang, H.; Han, G. Near-Infrared Light Activated Persistent Luminescence Nanoparticles *via* Upconversion. *Nano Res.* **2017**, *10*, 1840–1846.

(27) Fu, X.; Liu, C.; Shi, J.; Man, H.; Xu, J.; Zhang, H. Long Persistent Near Infrared Luminescence Nanoprobes $LiGa_5O_8:Cr^{3+}$–PEG–OCH_3 for *In Vivo* Imaging. *Opt. Mater.* **2014**, *36*, 1792–1797.

(28) Abdukayum, A.; Yang, C. X.; Zhao, Q.; Chen, J. T.; Dong, L. X.; Yan, X. P. Gadolinium Complexes Functionalized Persistent Luminescent Nanoparticles as a Multimodal Probe for Near–Infrared Luminescence and Magnetic Resonance Imaging *In Vivo*. *Anal. Chem.* **2014**, *86*, 4096–4101.

(29) Shi, J.; Sun, X.; Zhu, J.; Li, J.; Zhang, H. One–Step Synthesis of Amino-Functionalized Ultrasmall Near Infrared–Emitting Persistent Luminescent Nanoparticles for *In Vitro* and *In Vivo* Bioimaging. *Nanoscale* **2016**, *8*, 9798–9804.

(30) Maldiney, T.; Lecointre, A.; Viana, B.; Bessière, A. l.; Bessodes, M.; Gourier, D.; Richard, C.; Scherman, D. Controlling Electron Trap Depth to Enhance Optical Properties of Persistent Luminescence Nanoparticles for *In Vivo* Imaging. *J. Am. Chem. Soc.* **2011**, *133*, 11810–11815.

(31) Abdukayum, A.; Chen, J. T.; Zhao, Q.; Yan, X. P. Functional Near Infrared–Emitting Cr^{3+}/Pr^{3+} Co–Doped Zinc Gallogermanate Persistent Luminescent Nanoparticles with Superlong Afterglow for *In Vivo* Targeted Bioimaging. *J. Am. Chem. Soc.* **2013**, *135*, 14125–14133.

(32) Lécuyer, T.; Teston, E.; Ramirez-Garcia, G.; Maldiney, T.; Viana, B.; Seguin, J.; Mignet, N.; Scherman, D.; Richard, C. Chemically Engineered Persistent Luminescence Nanoprobes for Bioimaging. *Theranostics* **2016**, *6*, 2488–2524.

(33) Wang, J.; Ma, Q. Q.; Wang, Y. Q.; Shen, H. J.; Yuan, Q. Recent Progress in Biomedical Applications of Persistent Luminescence Nanoparticles. *Nanoscale* **2017**, *9*, 6204–6218.

(34) Maldiney, T.; Bessière, A.; Seguin, J.; Teston, E.; Sharma, S. K.; Viana, B.; Bos, A. J.; Dorenbos, P.; Bessodes, M.; Gourier, D. *et al.* The *In Vivo* Activation of Persistent Nanophosphors for Optical Imaging of Vascularization, Tumours and Grafted Cells. *Nat. Mater.* **2014**, *13*, 418–426.

(35) Li, Z.; Zhang, Y.; Wu, X.; Huang, L.; Li, D.; Fan, W.; Han, G. Direct Aqueous–Phase Synthesis of Sub-10 nm "Luminous Pearls" with Enhanced *In Vivo* Renewable Near–Infrared Persistent Luminescence. *J. Am. Chem. Soc.* **2015**, *137*, 5304–5307.

(36) Sun, M.; Li, Z. J.; Liu, C. L.; Fu, H. X.; Shen, J. S.; Zhang, H. W. Persistent Luminescent Nanoparticles for Super–Long Time *In Vivo* and *In Situ* Imaging with Repeatable Excitation. *J. Lumin.* **2014**, *145*, 838–842.

(37) Teston, E.; Richard, S.; Maldiney, T.; Lièvre, N.; Wang, G. Y.; Motte, L.; Richard, C.; Lalatonne, Y. Non-Aqueous Sol–Gel Synthesis of Ultra Small Persistent Luminescence Nanoparticles for Near–Infrared *In Vivo* Imaging. *Chem. - Eur. J.* **2015**, *21*, 7350–7354.

(38) Srivastava, B. B.; Kuang, A.; Mao, Y. B. Persistent Luminescent Sub-10 nm Cr Doped $ZnGa_2O_4$ Nanoparticles by a Biphasic Synthesis Route. *Chem. Commun.* **2015**, *51*, 7372–7375.

(39) Bessière, A.; Jacquart, S.; Priolkar, K.; Lecointre, A.; Viana, B.; Gourier, D. $ZnGa_2O_4:Cr^{3+}$: a New Red Long–Lasting Phosphor with High Brightness. *Opt. Express* **2011**, *19*, 10131–10137.

(40) Gourier, D.; Bessière, A.; Sharma, S. K.; Binet, L.; Viana, B.; Basavaraju, N.; Priolkar, K. R. Origin of the Visible Light Induced Persistent Luminescence of Cr^{3+}–Doped Zinc Gallate. *J. Phys. Chem. Solids* **2014**, *75*, 826–837.

(41) Tang, L.; Yang, X.; Dobrucki, L. W.; Chaudhury, I.; Yin, Q.; Yao, C.; Lezmi, S.; Helferich, W. G.; Fan, T. M.; Cheng, J. Aptamer–Functionalized, Ultra–Small, Monodisperse Silica Nanoconjugates for Targeted Dual–Modal Imaging of Lymph Nodes with Metastatic Tumors. *Angew.Chem. Int. Ed.* **2012**, *51*, 12721–12726.

(42) Tan, W.; Donovan, M. J.; Jiang, J. Aptamers from Cell–Based Selection for Bioanalytical Applications. *Chem. Rev.* **2013**, *113*, 2842–2862.

(43) Meng, H. M.; Fu, T.; Zhang, X. B.; Tan, W. Cell–SELEX-Based Aptamer–Conjugated Nanomaterials for Cancer Diagnosis and Therapy. *Natl. Sci. Rev.* **2015**, *2*, 71–84.

(44) Li, L. L.; Yin, Q.; Cheng, J.; Lu, Y. Polyvalent Mesoporous Silica Nanoparticle–Aptamer Bioconjugates Target Breast Cancer Cells. *Adv. Healthcare Mater.* **2012**, *1*, 567–572.

(45) Yuan, Q.; Wu, Y.; Wang, J.; Lu, D.; Zhao, Z.; Liu, T.; Zhang, X.; Tan, W. Targeted Bioimaging and Photodynamic Therapy Nanoplatform Using an Aptamer–Guided G–Quadruplex DNA Carrier and Near–Infrared Light. *Angew. Chem. Int. Ed.* **2013**, *52*, 13965 – 13969.

Table of Contents Graphic